

# Laser Transmission Welding of Thermoplastics—Part I: Temperature and Pressure Modeling

**James D. Van de Ven**  
e-mail: vandeven@me.umn.edu

**Arthur G. Erdman**  
e-mail: agerdman@me.umn.edu

Mechanical Engineering Department,  
University of Minnesota,  
111 Church Street SE,  
Minneapolis, MN 55455

*This paper discusses the development of a model of laser transmission welding that can be used as an analytical design tool. Currently the majority of laser transmission welding (LTW) applications rely on trial and error to develop appropriate process parameters. A more rigorous design approach is not commonly used primarily due to the complexity of laser welding, where small material or process parameter changes can greatly affect the weld quality. The model developed in this paper also enables optimizing operating parameters while providing monetary and time saving benefits. The model is created from first principles of heat transfer and utilizes contact conduction that is a function of temperature and pressure, Gaussian laser distribution, and many material properties that vary with temperature including the absorption coefficient. The model is demonstrated through a design example of a joint between two polyvinyl chloride parts. The model is then validated with samples welded with a diode laser system using the operating parameters developed in a design example. Using the weld width as the primary output, the error between the model and the experimental results is 4.3%, demonstrating the accuracy of the model. [DOI: 10.1115/1.2752527]*

*Keywords:* laser welding, modeling, PVC

## Background

Several laser transmission welding (LTW) models of varying complexities have been presented in the literature. Generally the models poorly correlate to experimental data and various correction factors have been used to improve the fit. Creating a robust model of LTW is difficult due to the very rapid heating and high temperature gradients, requirement for accurate optical properties, and the variability of material properties with temperature.

One of the first analytical models of LTW, presented in 1999, provided important information about the energy distribution of the laser beam after passing through the “transparent” material. Measuring the light intensity at prescribed locations behind a “transparent” PA6 specimen with a moving light energy detector yielded a Gaussian energy distribution, which was symmetric about the central axis of the laser [1].

Further work modeling the laser intensity profile behind a “transparent” thermoplastic part was presented in 2002 where equations for the laser intensity, which could be used in a numerical model of the heating phase, were presented. When calculating the total power from the incremental power measurements, a correction factor between 1.3 and 1.5 was necessary to obtain agreement. Presented in this work is also a relationship between the absorption coefficient and temperature, which was used to create better agreement between the model and experimental data [2]. Using this background information, a two-dimensional finite element model of the joining process was also constructed and presented [3].

More intensive modeling efforts at the University of Paderborn were presented in 2004. In one of these efforts, a two-dimensional finite element model was used to not only predict the temperature distribution as a function of time during welding, but also the

material flow due to clamping pressure and thermal expansion. In this work the energy distribution of the laser was simplified from a Gaussian distribution to two grades of laser intensity of 3 W/mm<sup>2</sup> and 1.8 W/mm<sup>2</sup>. This work assumed perfect thermal contact between the two components being joined, resulting in optimal heating. The maximum temperature in this simulation occurred along the central axis of the laser approximately 0.1–0.2 mm into the core of the “absorbing” part. When modeling the material flow the use of a specific joining pressure lead to convergence problems. Instead, their model used a joining displacement as a function of time [4,5].

Two notable LTW models were presented in 2002. Researchers at Tokyo Institute for Technology published a paper documenting their work creating a two-dimensional numerical heating phase model. This model assumed a steady-state condition and did not include transients as in the work at the University of Paderborn [6]. A second heat transfer simulation modeled the use of the absorbent ink Clearweld. In this case, a weld is created between two otherwise “transparent” materials [7]. Both this model and that by Sato et al. assumed the material properties, including the absorption coefficient, to be a constant, and not a function of the temperature.

One model that did demonstrate good agreement with the experimental results was presented by Grewell and Benatar in 2006. This model predicts the size of microwelds, on the order of 50–250 μm. This model includes molecular diffusion and squeeze flow, but did not include variable absorption coefficient or account for the contact conduction between the joined parts [8].

## LTW Process Fundamentals

Fundamental laws of heat transfer along with optical, mechanical, and thermal properties of solids are used in the model to understand the basics of LTW using the contour welding method. During LTW, a focused laser beam is directed at two overlapping thermoplastic parts. The first part contacted by the laser beam is designed to be primarily transparent, and thus is labeled the

Contributed by the Manufacturing Engineering Division of ASME for publication in the JOURNAL OF MANUFACTURING SCIENCE AND ENGINEERING. Manuscript received May 31, 2006; final manuscript received April 17, 2007. Review conducted by Y. Lawrence Yao.

“transparent” part. Likewise, the second part is designed to absorb the laser radiation and is thus labeled the “absorbing” part.

As the laser beam strikes the surface of the “transparent” part, a fraction of the incident light is reflected and the remaining light energy enters the bulk of the material. While the majority of the light entering the “transparent” part is transmitted through the material, with the possibility of significant scattering, a portion of the energy is absorbed. Light absorption within a solid can be described by Beer’s law [9]

$$I(z) = I_0 e^{-\alpha z} \quad (1)$$

where  $I(z)$  is the optical intensity as a function of material depth;  $I_0$  is the optical intensity at  $z=0$ ;  $\alpha$  is the absorption coefficient; and  $z$  is the material depth. The absorption coefficient was experimentally determined for clear PVC at ambient temperatures and at elevated temperatures [10,11].

The laser light that is transmitted through the “transparent” material strikes the surface of the “absorbing” material, where a fraction of the energy is reflected and the remaining energy enters the bulk of the material. The absorption of the laser light in the “absorbing” material can again be described using Beer’s law. Depending on the thickness and absorption coefficient of the “absorbing” material, a portion of the laser energy may transmit completely through both parts.

The laser energy in the near-infrared spectrum that is absorbed in a thermoplastic causes vibration of electron bonds [9]. This bond vibration causes localized heating of the material. Using the laws of heat transfer, this heat is conducted within and between both parts and transferred to the surroundings through convection and radiation. When heated to temperatures above the melting point, or melting range, the thermoplastic enters a liquid form, allowing a joint to be formed. Heating the material also increases the internal pressure due to thermal expansion, assuming no displacement of the two parts is allowed. This pressure further improves the interaction of the melted polymer layers of the two parts.

Contour welding involves relative motion between the laser beam and the thermoplastic parts in a direction perpendicular to the beam of the laser. This movement allows a continuously operating laser beam to irradiate a line of a specific width, heating the materials at the part interface into the melting range. Continued movement along the weld seam allows the heated polymer to cool and form a joint. Upon reaching the end of the joint, the laser power can be terminated or a second pass of the laser over the material, next to the first weld seam, can be used to create a wider weld.

## LTW Model Description

Due to the complexity of LTW and the desire for a solution that allows a great deal of flexibility in process parameters and part geometry, a numerical model was employed. The model predicts both the internal temperature and pressure of the two materials and is based on first principles of heat transfer. It is designed to allow easy modification of operating parameters.

While a commercially available finite-element package could be used to model the LTW process, there are certain advantages of developing a model from first principles. The primary reason to create a model from first principles is that all assumptions made by the model are known. Second, creating a model allows for greater flexibility in implementing complex properties. For example, the changing absorption coefficient as a function of temperature can be easily implemented into a proprietary code, while it would be more difficult with a commercial package. The mathematical model is programmed in the software MATLAB, a product of MathWorks.

A detailed design of a laser welded joint requires information about the width of the melt pool and the temperature distribution into the materials, along the axis of the laser. To satisfy this need, a two-dimensional model was developed where the first dimen-

sion is into the material and the second dimension is perpendicular to the path of the laser. The two-dimensional simplification neglects the heat transfer in the direction of laser travel and is valid for the short heating times and poor thermal conductivity of plastics. To simplify equations, the distance between the nodes is the same along both axes, creating a square mesh.

The laser energy absorbed in the two materials is represented with a heat generation term. Rewriting Beer’s Law, Eq. (1), allows solving for the transmission fraction and therefore the power density as follows

$$T = \frac{I(z)}{I_0} = e^{-\alpha z} \quad (\text{unitless}) \quad (2)$$

$$\frac{I_{\text{out}}}{I_{\text{in}}} = e^{-\alpha \Delta z} \quad (\text{unitless}) \quad (3)$$

$$I_{\text{out}} = I_{\text{in}} e^{-\alpha \Delta z} \quad (\text{W/m}^2) \quad (4)$$

where  $T$  is the transmission fraction;  $I_{\text{out}}$  is the power density leaving a volume element;  $I_{\text{in}}$  is the power entering a volume element; and  $\Delta z$  is distance between the nodes along the  $z$  axis, which is the axis into the material. The heat generation in a specific volume element becomes

$$\dot{g} = \frac{I_{\text{in}} - I_{\text{out}}}{\Delta x} \quad (\text{W/m}^3) \quad (5)$$

where  $\dot{g}$  is the heat generation per unit volume. The laser power density entering the next volume element becomes the power density exiting the previous volume element. The fraction of light energy reflected from the surface of each material is also subtracted from the power density at each surface element.

Through an experimental method, the optical intensity across the beam of a 30 W, 808 nm fiber coupled diode laser was measured using a systematic scanning process. By placing a photodiode behind a 1-mm-diameter hole in a flat plate, a portion of the laser beam could be measured. A data acquisition system was used to record the light intensity reaching the photodiode, which was attenuated by a 1.0 optical density filter. By scanning the laser beam across the plate repeatedly, moving 0.5 mm perpendicular to the scan between each pass, the intensity distribution was recorded. Compiling this data produces the plot found in Fig. 1. Using the center of the beam as a reference, the power intensity measurements were averaged in groups according to the distance from the beam center. These averaged values are well fit by a Gaussian curve, as seen in Fig. 2.

As demonstrated by Becker [3], a numerical integration can be performed across the beam using the Gaussian fit to calculate the total laser power. The Gaussian fit equation, such as  $I = 9795.7e^{-87000r^2}$  can be written generally as

$$I(r) = ae^{-br^2} \quad (6)$$

The total power can be found by integrating in polar coordinates as follows

$$P_{\text{tot}} = \int_0^R \int_0^{2\pi} I(r)r \cdot d\theta \cdot dr \quad (7)$$

Substituting in the general function for  $I(r)$

$$P_{\text{tot}} = \int_0^R \int_0^{2\pi} are^{-br^2} \cdot d\theta \cdot dr \quad (8)$$

$$P_{\text{tot}} = \int_0^R 2\pi are^{-br^2} \cdot dr \quad (9)$$

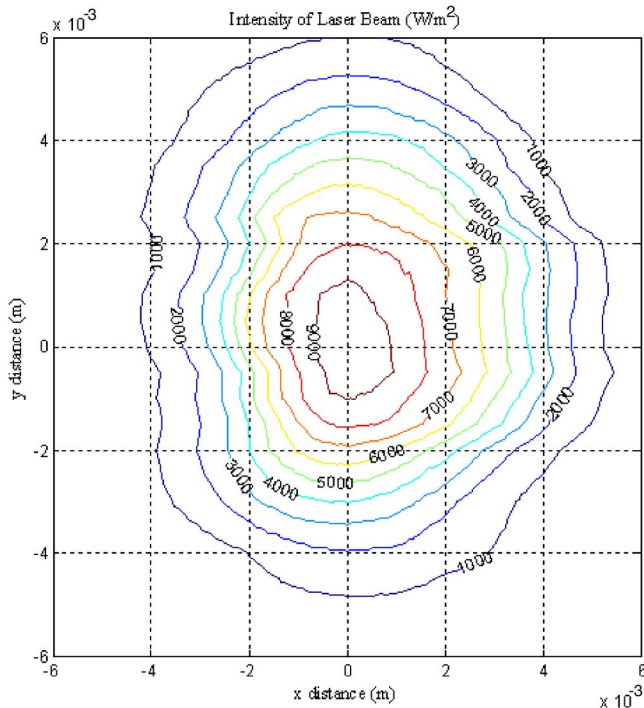


Fig. 1 Power intensity of the laser beam computed by scanning over a 1-mm-diameter hole

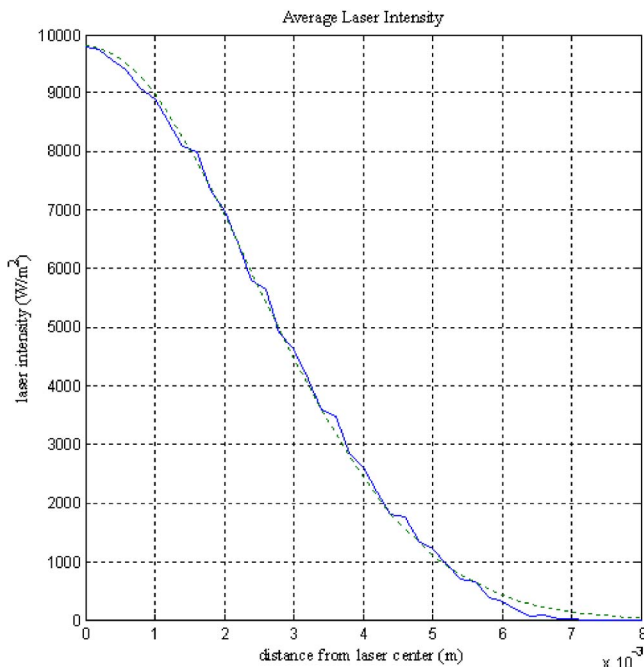


Fig. 2 Average power intensity of the laser beam as a function of distance from the center of the beam. The slightly jagged (blue) line is the averaged power intensity and the smoother (dashed green) line is a Gaussian curve fit to the data. The equation of the Gaussian fit line is:  $I = 9795.7e^{-87000r^2}$ , where  $I$  is the power intensity ( $W/m^2$ ) and  $r$  is the radial distance from the center of the beam (m). Note that these values need to be divided by the transmission index of the optical density filter to yield the actual beam intensity.

$$P_{\text{tot}} = 2\pi a \frac{-1}{2b} \int_0^{-bR^2} e^u \cdot du \quad (10)$$

where  $u = -br^2$  and  $du = -2br$

$$P_{\text{tot}} = \pi \frac{a}{b} (1 - e^{-bR^2}) \quad (11)$$

As  $R \rightarrow \infty$

$$P_{\text{tot}} = \pi \frac{a}{b} \quad (12)$$

The optical power of the diode laser was also measured directly using a power meter. It should be noted that the integrated power using the scanning method was lower than obtained using the power meter at the four different power levels investigated. As was found by Becker [3], a coefficient of approximately 1.5–1.6 was needed to create agreement. For this reason, the laser power used for the model and discussion is from measurements with the laser power meter. Similarly, the beam distribution used in the model and discussion is from the scanning method.

The structure for this model is as follows: two materials, which are modeled as semi-infinite plates, are brought into contact. The first material, labeled Material B, is highly transparent to near-infrared radiation, while the second material, labeled Material C, is highly absorptive of near-infrared radiation. The laser beam is centered on the top row of nodes, shown in Fig. 3, thus allowing the calculations to be simplified by creating a mirror boundary condition. The lower boundary condition, also seen in Fig. 3, is controlled at a constant temperature, which is valid for samples significantly wider than the laser beam diameter and short time periods.

The heat transfer components present in the model include: radiation from the top and bottom external material surfaces to the surroundings, convection from the top and bottom external material surfaces to the surrounding air, conduction within each material, heat generation within each material from the laser absorption, thermal contact conduction between the two materials, and light reflection at both surfaces (Fig. 3).

Because the intensity of the laser beam follows a Gaussian distribution and the beam diameter is variable, the distance between each surface node and the center of the laser beam is required. To aid in calculating this distance, Fig. 4 is constructed by rotating Fig. 3 +90 deg about the  $x$  axis. Based on the laser velocity,  $v$ , the time increment,  $\Delta t$ , and the number of time steps, the distance in the  $y$  direction between the center of the laser beam and the origin of the  $x, y, z$  coordinate system is found. Using this distance in the  $y$  direction and the distance of each node in the  $x$  direction from the origin, the distance from the laser center is calculated. Entering this distance into the Gaussian fit of the laser distribution, the incident laser power reaching each surface node is calculated.

The heat transfer model is a numerical approximation using the energy balance method. This method divides a medium into a large number of volume elements and then performs an energy balance on each element. Each volume element is represented by a node at its center, where the temperature is determined. Contained within the two-dimensional mesh described above are 18 unique nodal conditions based on the boundary conditions and in which of the two materials the node resides.

The most frequently occurring nodal condition resides within the bulk of the two materials. These interior nodes experience conduction from all the surrounding nodes and have the possibility of heat generation within the node due to the absorption of laser radiation as previously discussed. Performing an energy balance for an interior node:

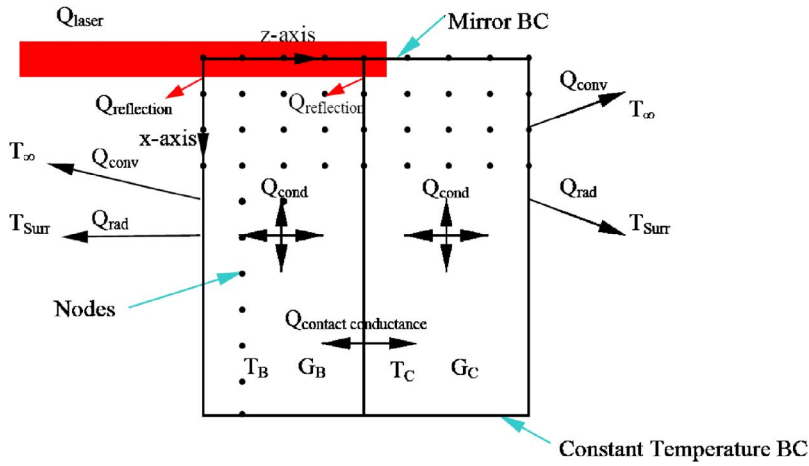


**Fig. 3** Heat transfer components of the two-dimensional numerical model. Material B is the “transparent” part and Material C is the “absorbing” part. In this view, the laser beam is collinear with the positive  $z$  axis and is traveling into the paper in the direction of the positive  $y$  axis (not labeled).

Heat transferred into the volume element during  $\Delta t$  + heat generated within the volume element during  $\Delta t$  = the change in energy content of the volume element during  $\Delta t$  which can mathematically be expressed as

$$\dot{Q}_{\text{cond, left}} + \dot{Q}_{\text{cond, top}} + \dot{Q}_{\text{cond, right}} + \dot{Q}_{\text{cond, bottom}} + \dot{G} = \frac{\Delta E}{\Delta t} \quad (13)$$

Noting that the distance between nodes is equal,  $\Delta x = \Delta z$ , and using a unit depth in the  $y$  direction, the area of any side of the volume element is:  $A = \Delta x \cdot 1 = \Delta z \cdot 1$ . In addition, the change in energy of the volume element can be expressed as

$$\Delta E = mC\Delta T = \rho V_{\text{element}} C \Delta T \quad (14)$$

where  $m$  is the mass of the volume element;  $C$  is the specific heat;  $\Delta T$  is the change in temperature during  $\Delta t$ ;  $\rho$  is the mass density; and  $V_{\text{element}}$  is the volume of the element. Using Fig. 5, Eqs. (13) and (14) can be combined to form

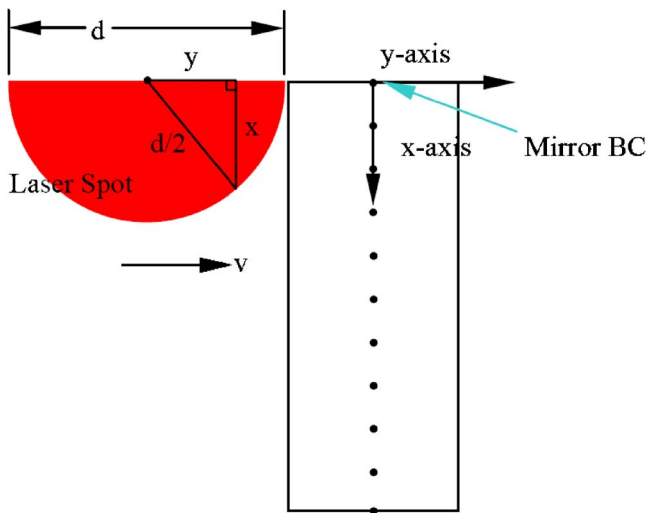


**Fig. 4** Laser spot approaching the nodes on the surface of the  $x$ - $y$  plane. This diagram is formed by rotating Fig. 3 +90 deg about the  $x$  axis. For reference, the  $z$  axis is pointing out of the paper. Using this diagram the number of nodes along the  $x$  axis that are within the laser beam can be calculated.

$$kA \frac{T_{m-1,n} - T_{m,n}}{\Delta z} + kA \frac{T_{m,n-1} - T_{m,n}}{\Delta x} + kA \frac{T_{m+1,n} - T_{m,n}}{\Delta z} + kA \frac{T_{m,n+1} - T_{m,n}}{\Delta x} + \dot{g}_{m,n} V_{\text{element}} = \rho V_{\text{element}} C \frac{T_{m,n}^{i+1} - T_{m,n}^i}{\Delta t} \quad (15)$$

Simplifying, this equation yields

$$k(T_{m-1,n} + T_{m,n-1} + T_{m+1,n} + T_{m,n+1} - 4T_{m,n}) + \dot{g}_{m,n} \Delta x^2 = \rho \Delta x^2 C \frac{T_{m,n}^{i+1} - T_{m,n}^i}{\Delta t} \quad (16)$$

where  $k$  is the thermal conductivity and  $T_{m,n}^i$  and  $T_{m,n}^{i+1}$  are the temperature of the central node at the current and next time steps, respectively. The system is then solved explicitly for the temperature at the next time step

$$T_{m,n}^{i+1} = \frac{k\Delta t}{\rho \Delta x^2 C} (T_{m-1,n} + T_{m,n-1} + T_{m+1,n} + T_{m,n+1} - 4T_{m,n}) + \frac{\dot{g}_{m,n} \Delta t}{\rho C} + T_{m,n}^i \quad (17)$$

The explicit method of solving allows the nodal temperatures to

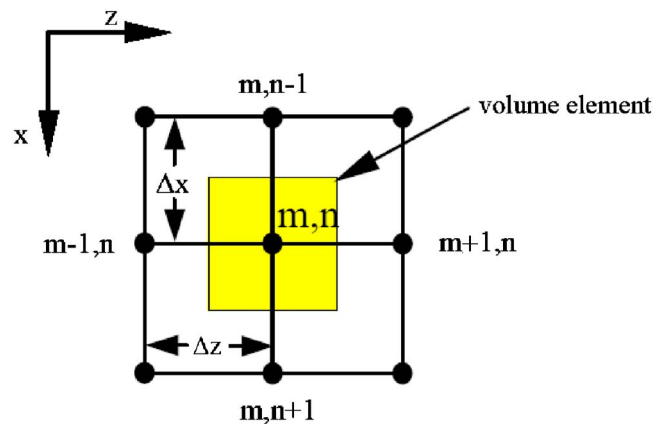


**Fig. 5** A volume element contained within the interior of one of the two parts. The four surrounding nodes are labeled to aid in the heat transfer equations. Note that the mesh is square allowing  $\Delta x = \Delta z$ .

be solved directly, without simultaneous equations, but limits the allowable time step size to maintain stability. The stability criterion for the explicit method requires that

$$\tau = \frac{k\Delta t}{\rho C\Delta x^2} \leq \frac{1}{2} \quad (18)$$

where  $\tau$  is the mesh Fourier number;  $\Delta t$  is the time step;  $\rho$  is the mass density;  $C$  is the specific heat; and  $\Delta x$  is the distance step [12]. The limits established by the stability criterion are not a problem for this model as the welding process is rapid and small time steps are desirable to improve the accuracy. As will be discussed later, material properties, including the thermal conductivity and the specific heat, which are used to calculate the mesh Fourier equation, do change with temperature. Therefore, the stability criterion needs to be checked across the temperature range of expected operation.

The 17 other nodal conditions are solved in the same manner, yet have different boundary conditions. The nodes at the exterior edges of both materials represent volume elements that are 1/2 the volume of the central elements, while the corner nodes represent volume elements with 1/4 the volume of the central elements. On the outer sides of the two parts, convection and radiation to the surrounds is modeled in place of one of the conduction terms. The uppermost nodes have a mirror boundary condition meaning that the conduction from the above term is replaced by doubling the conduction from below the term. The lowermost nodes are fixed at a constant ambient temperature. Finally, the nodes at the interface of the two materials occupy 1/2 the volume of the interior nodes and have a contact conduction term from the adjoining part. The thermal contact conduction boundary condition will be explained further in the following section. In the interest of avoiding tedium, the derivation of the 17 other nodal conditions will not be presented.

Within the model are a number of material properties that vary with temperature. Among these properties are the absorption coefficient, thermal conductivity, heat capacity, contact conduction, elastic modulus, and specific volume. To manage these varying properties, lookup tables were created and stored in separate data files. Throughout the simulation, the program uses these lookup tables and linear interpolation to find the material properties appropriate for the current node temperature. Further discussion of the material properties is presented in the next section of this paper.

In addition to the temperature distribution throughout the material, the internal pressure is also of interest. Pressure is created by both external fixturing and by thermal expansion of the two materials during the welding process. Previous experimental work found that the pressure was not a significant factor in contour welding, as long as excessive limits were not exceeded [11,13]. In light of this information, a simplified method is used to calculate the pressure within the two materials during welding.

Instead of creating a full finite-element-method approximation of the pressure, a one-dimensional approach is used. Making the assumption that the nodes along the axis of clamping have the largest effect on the pressure and that heating in the  $x$  direction within the weld zone is relatively uniform, a one-dimensional calculation in the  $z$  direction provides an adequate rough estimate of the pressure. The outer surfaces of the two materials are set to a fixed position, which is reached after an initial clamping pressure is applied. The elements between the two surfaces combine to form a statically indeterminate axial-loaded member. By balancing the expansion due to thermal effects in each element with the contraction due to the fixed outer surfaces, the pressure can be calculated. This calculation uses both the specific volume and the modulus of elasticity, which are both functions of temperature.

Using this same method, the issue of gaps between the two parts can be explored. Through heating the two materials, gaps between the two parts will decrease until the parts make contact and pressure begins to increase. Accounting for gaps is critical to

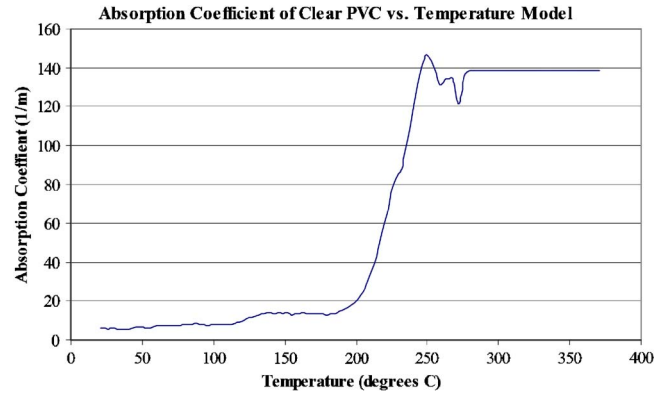


Fig. 6 Absorption coefficient of clear PVC as a function of temperature. Note that the values above 550 K are predicted values.

the heat transfer mechanisms of LTW. When a gap exists between the parts, the contact conduction is negligible, limiting the heat transfer between the “absorbing” part and the “transparent” part.

## Material Properties

Accurate material properties are vital to a precise LTW model. A fundamentally sound model will provide erroneous results when supplied with incorrect material property information. For this reason, this section of the paper discusses the more complex material properties of clear PVC. These properties have been gathered from the literature, handbooks, and experimentally.

The absorption coefficient is one of the most important properties used in the model because it determines where and to what degree the laser energy is absorbed. Previous experimental work with clear polyvinyl chloride (PVC) found that the absorption coefficient is a function of the temperature [11]. From ambient temperature to the beginning of the melt phase, the absorption coefficient remains relatively constant. Through the melt phase the absorption coefficient rapidly increases before reaching a subsequent plateau. A plot of the absorption coefficient of the “transparent” part as a function of temperature can be found in Fig. 6 [11]. It should be noted that little scattering of the laser beam is expected as the PVC is amorphous.

The absorption coefficient of the “absorbing” part is also very important for modeling. The light transmission and reflection of a gray pigmented PVC were measured using previously developed techniques in an optical black box [10]. The light transmitted through a 0.284 mm (0.0112 in.) sample was found to be 0.07% of the incident radiation. It is expected that the absorption coefficient of the “absorbing” part will vary with temperature similar to the clear PVC part. However, because the absorption coefficient of the “absorptive” part is quite high at  $25,536 \text{ m}^{-1}$ , it was decided that increases from this value would not significantly affect the simulation.

When calculating the force created by material deflection, as in the case of thermal expansion, the elastic modulus of a material is needed. The elastic modulus decreases with increasing temperature, demonstrated by the polymer softening significantly above the glass transition temperature. Two sources of experimental data relating temperature and the elastic modulus of PVC provided similar results [14,15]. To use the elastic modulus in the mathematical model, values were fitted to these experimental data and entered into a “lookup” table. These fitted values are shown in Fig. 7.

The specific heat is used to determine how quickly a material will be heated by a given energy source, in this case, the laser beam. The specific heat values used in the model, stored in the

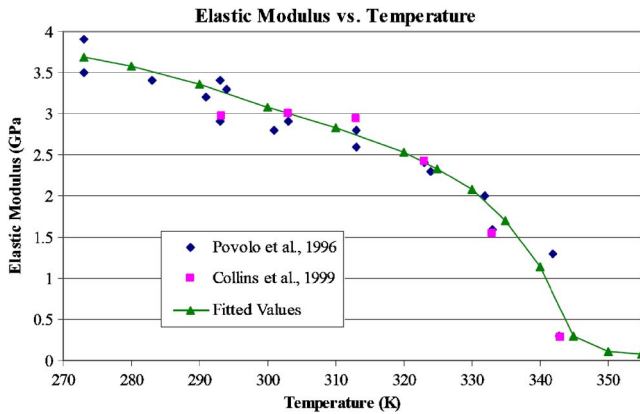


Fig. 7 Elastic modulus of PVC from two different sources and the values fit for the model

form of a lookup table, were calculated from a table of thermal diffusivity values with knowledge of the thermal conductivity and mass density [14]. These variable are related by

$$\alpha = \frac{k}{\rho C} \quad (19)$$

where  $\alpha$  is the thermal diffusivity (not the absorption coefficient as used previously);  $k$  is the thermal conductivity;  $\rho$  is the mass density; and  $C$  is the specific heat [12]. This equation can then be solved for the specific heat, yielding the values found in Table 1.

When a material is clamped in a position and simultaneously heated, internal pressure is developed due to the thermal strain that must be reacted. The relationship between the change in temperature of a material and the change in length is often described by the coefficient of thermal expansion. When heating a polymer from a solid through the melting phase, the thermal expansion is no longer a constant. Another way of describing the volume of a material as a function of temperature is the inverse of the density, the specific volume (Table 2) [16]. By knowing the unrestrained volumetric change of a specified mass of a material due to heating, the internal pressure can be calculated.

Thermal conductivity is of prime importance to any heat transfer problem as it defines the conduction of heat and thus the temperature difference throughout a material. The thermal conductivity of PVC varies with temperature, from 0.160 W/m/K at room temperature to a plateau of 0.165 W/m/K at 373 K [14]. While the total variation is quite small, at approximately 3%, it was included for completeness.

Table 1 Specific heat as a function of temperature. Note that the values found in this table were calculated from the thermal diffusivity with knowledge of the thermal conductivity and mass density.

Specific Heat  
Source: Collins et al., 1999

Temperature (K)	Specific Heat (J/kg/K)
293	957.41
300	972.1
320	1051.3
340	1167.8
352	1297.7
360	1427.9
380	1616.8
400	1730.7

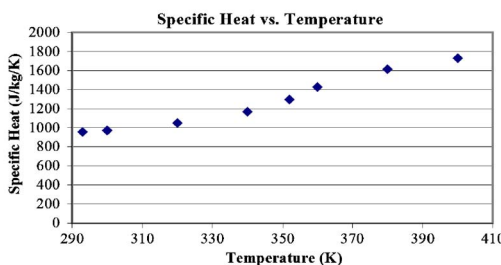
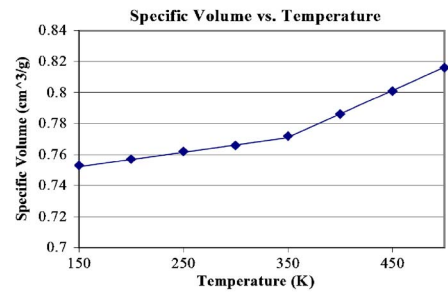


Table 2 Specific volume of PVC as a function of temperature. Note the two constant slope sections of the plot, which are split at the inflection point at the glass-transition temperature.

Specific Volume  
Source: Abu-Sharkh, 2001

Temperature (K)	Specific Volume (cm <sup>3</sup> /g)	Specific Volume (m <sup>3</sup> /kg)
150	0.753	0.00075
200	0.757	0.00076
250	0.762	0.00076
300	0.766	0.00077
350	0.772	0.00077
400	0.786	0.00079
450	0.801	0.0008
500	0.816	0.00082



The issue of contact conduction has been downplayed by most LTW research. Work at the University of Paderborn has assumed perfect contact between the two materials, allowing optimal heat transfer between the two parts [4]. The author is unaware of any LTW models that directly apply contact conduction.

The thermal contact conduction boundary condition is extremely important to LTW. By principle, LTW relies on the conduction of heat from the surface of the “absorbing” part to the mating surface of the “transmissive” part, allowing melting to occur in both materials. Regardless of the apparent uniformity of the joined surfaces, microscopic roughness will exist that impedes the heat conduction [12]. Understanding this impedance is critical for modeling.

The contact conduction is not trivial to estimate for a specific joint as it depends on the surface roughness, clamping pressure, and the modulus of elasticity. Numerous experimental studies are presented in the literature on the topic of contact conduction between polymers and metals in the field of injection molding. These findings cannot be directly applied to polymer-to-polymer joints due to different material properties. A model based on microscopic elastic deformation allows one to calculate the thermal contact conductance as a function of the material and joint properties [17]. This model can be written as

$$h_c = \frac{1.49km_{ab}}{R} * \left( \frac{2.3P}{Em_{ab}} \right)^{0.935} \quad (20)$$

where  $h_c$  is the contact conductance (W/m<sup>2</sup>/K);  $k$  is the thermal conductivity (W/m/K);  $m_{ab}$  is the mean asperity slope (radians);  $R$  is the root mean square of the surface roughness (m);  $P$  is the joining pressure (Pa); and  $E$  is the elastic modulus (Pa). The constant 1.49 and the power 0.935 come from solving a system of equations involving the complementary error function. The constant 2.3 arises from an experimental investigation of the surface contact area of two plates relating to the applied load [17].

Studying Eq. (20) and implementing it in the model realizes an interesting occurrence. The variables within the equation that change during the laser welding process include the thermal conductivity, the internal pressure, and the elastic modulus. The change in the thermal conductivity is fairly minimal, so it will be disregarded momentarily. As the surface of the “absorbing” material increases in temperature due to the absorption of laser radiation, it begins to expand and increase the joining pressure. When the material temperature rises, the elastic modulus also decreases. Both of these factors increase the thermal contact conductance, increasing the heat transfer to the “transmissive” part. As the temperature of the “transmissive” part elevates, not only is the thermal contact conduction further increased, the absorption coefficient also increases, changing the distribution of laser absorption. The results are that the “absorbing” material is first rapidly heated

due to the relatively low contact conduction. The contact conduction then rapidly increases and the temperature of the two surfaces approach similar values.

From Eq. (20) it can also be noted that when the joining pressure drops to zero, as occurs when a gap is present, the contact conductance also becomes zero. This equation is based on the assumption of operating in a vacuum, yet is a valid approximation due to the very low convective heat transfer that occurs with air as a medium. This is the reason that bridging gaps is very difficult in laser welding as only the “absorbing” material is heated and expands to close the gap.

### Design Example

To demonstrate the model and how it is used to design a LTW joint, the results of a short design example are presented. An infinite number of LTW joint specifications exist including variations in joint geometry, materials, and the desired weld outcome. For this example a general case is selected.

The example joint will consist of two 127 mm (5 in.) long by 25 mm (1 in.) wide by 3.2 mm (0.125 in.) thick PVC parts, one clear and the other gray. The clear part will be placed on top of the gray part and clamps will be available to apply pressure to the two materials. A 2.5-mm-wide weld seam is desired between the two materials. The available diode laser is fiber coupled and operates at a wavelength of 808 nm with a maximum power output at the focusing optic of 30 W.

Through an iterative design process the model is used to shape the process parameters to achieve the desired weld characteristics. Evaluation of each iterative trial involves assessing the weld width based on the temperature profile in the weld zone, the pressure within the weld zone, and the maximum temperature within the two materials. Based on these criteria, the input parameters in the following iteration are modified to closer align the model outcome with the desired results.

The iterative design method resulted in a successful solution for the joint example. The input parameters for this solution include an initial clamping pressure of 2 MPa (218 psi); a surface roughness of 1.8  $\mu\text{m}$ ; a 5.7 mm laser beam diameter; 17 W of laser power; and a welding velocity of 0.06 m/s (2.4 in./s). Three parameters that greatly affect the computation time are the distance between nodes, the time step, and the run time. For a faster yet coarser model, a time step of 1 ms, a distance between nodes of 0.1 mm, and a run time of 0.12 s are selected.

The first item of interest when running the model is to check for stability. As previously described, the explicit solving method requires that  $\tau$ , the mesh Fourier number, be less than 0.5; in this case it is 0.012 and thus will provide a stable solution. Running the model with the described input parameters on a Pentium 4 computer with a 2.8 GHz processor and 1.0 GB of RAM takes approximately 273 s of processing time.

Four output plots are used for the primary assessment of the model results. The first plot displays the temperature at the part interface as a function of time and width (in the  $x$  direction), allowing the weld width to be predicted. The second plot presents the internal pressure also as a function of the time and width. A third graph is used to plot the gap size, defined as the distance between the “transparent” and “absorptive” parts, across the width of the material as a function of temperature. The final plot displays the maximum temperature in the two materials as a function of the width, allowing possible thermal decomposition to be monitored. The four output plots from the design example solution can be found in Fig. 8.

Evaluating the output plots in Fig. 8 requires a relationship between temperature and weld formation. Previous experimental work with short-duration hot tool welding found that optimal welds were created at temperatures above approximately 485 K [18,19]. In Fig. 8 it visually appears that the weld width, defined as the width reaching a temperature above 485 K, is at least the

2.5 mm desired width. The reader will notice that the contour lines are rather jagged due to the relatively large time steps and distance steps. As the design solution is approached it is beneficial to begin improving the precision of the results by decreasing the distance between nodes and the duration of the time steps at the expense of added processing time. Repeating this refinement process multiple times also allows the convergence of the model to be verified.

The prime reason for interest in the convergence of a model is to ensure that as the distance between nodes and the duration of the time steps decreases, the model approaches a finite value. This is important as it ensures that results obtained with a coarse model provide a good approximation, which can be improved through more computationally intensive models. In other words, a model that converges on a finite value will always get closer and closer to that value as the step sizes are decreased.

Leveraging the parameters in the above design example, the maximum temperature at the interface of the two parts at a distance of 1.25 mm from the centerline will be set as the output of interest for the convergence study. Three more refinements of the step sizes will be presented, while maintaining all the same input parameters. The first refinement, labeled version 2, will decrease the distance step from 0.1 mm to 0.05 mm and the time step from 1 ms to 0.5 ms. The second refinement, labeled version 3, will further decrease the distance step from 0.05 mm to 0.02 mm and the time step from 0.5 ms to 0.3 ms. The final refinement, labeled version 4, will further decrease the time step to 0.2 ms while leaving the distance step at 0.02 mm. A contour plot from version 4 at the time of maximum heating width above 485 K can be found in Fig. 9.

To aid in assessing the convergence of the model, the maximum temperature of the node 1.25 mm from the weld centerline at the interface of the two parts was found for the four presented versions of the design example. These temperature values, the time step, the distance step, and the time of the maximum temperature in the four versions, can be found in Table 3. From the table it can be seen that as the step sizes are decreased, the deviations in maximum temperature decrease. In addition, the time at which the maximum temperature occurs at the described nodal location also converges on a single value.

The contour plot in Fig. 9 coincides with the time step that the maximum heated width above 485 K is achieved. From this plot one can observe that the highest temperature does in fact occur within the “absorbing” part. In addition, it can be observed that the temperature gradient within the “transparent” part in the width direction is large when approaching the edge of the weld. At the edge of the desired weld zone (width=1.25 mm), the temperature reaches 510.5 K, indicating that a successful weld is predicted. In fact, the width of heating above 485 K is 2.60 mm in width. The input parameters could be further refined to narrow this width to the 2.5 mm specified by the original problem statement. In the interest of brevity in this example problem, the depicted results will be considered the design solution.

It should also be noted that the designer should also be concerned with the decomposition of the material. Because of the vary rapid heating and cooling occurring during LTW, extreme temperatures can be reached without resulting in decomposition [3]. This is especially true of PVC due to its autocatalytic behavior [20].

### Experimental Verification

To validate the model samples were welded using a diode laser system and the parameters developed in the design example. Five samples were welded in a T-joint geometry (Fig. 10) with a 30 W, 808 nm diode laser coupled through a fiber optic cable to an  $x$ - $y$  gantry style table. The samples were machined from a PVC sheet with a measured surface roughness between 1.7 and 1.9  $\mu\text{m}$ . The

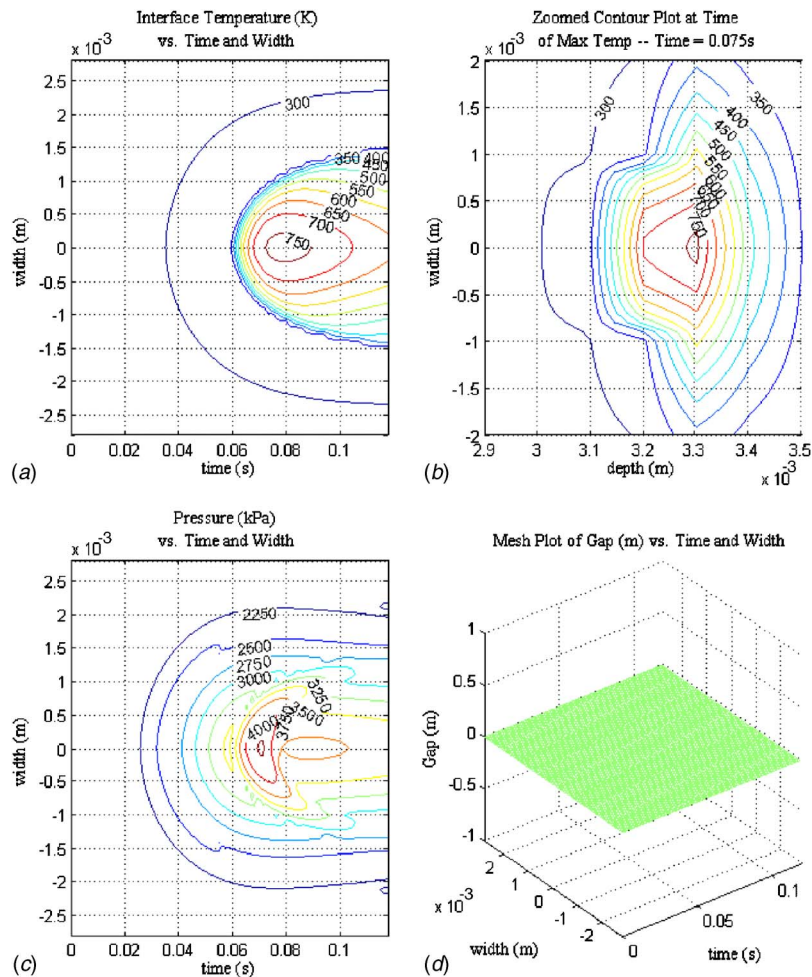


**Fig. 8** The four output plots of the model for the design solution. The plot in the upper left shows the temperature of the “transmissive” part at the interface of the two materials as a function of time and width. The plot in the upper right is a zoomed contour plot of the interface zone at the time step that the maximum temperature occurs. Note that in this case, the interface occurs at a depth= $3.2 \times 10^{-3}$  m. As can be seen, this maximum temperature typically occurs slightly below the surface of the “absorbing” part. The plot in the lower left shows the internal pressure as a function of time and width. Finally, the plot in the lower right shows the gap size along the width as a function of time. Note that the width dimension is along the  $x$  axis (Fig. 1 and 2) with a mirror boundary condition at  $x=0$ .

samples were welded at a velocity of 0.06 m/s, a laser output power of 17 W, a beam diameter of 5.7 mm, and a clamping pressure of 2 MPa.

The primary output from the mathematical model is the temperature distribution in the weld zone as a function of time. The best way to validate the model would be to directly measure the weld zone temperature during welding. Unfortunately, measuring this subsurface temperature is difficult.

One possible method of measuring the material temperature directly is through the use of a thermocouple or thermistor. Unfortunately, as discussed by Becker and Potente and demonstrated by Kennish et al., thermocouples will absorb the laser energy directly and not correctly read the temperature of the surrounding material [2,7]. In addition, placing an object in the weld zone that is in contact with both the “absorptive” and “transmissive” parts will likely affect the desired clamping pressure or even cause a gap between the two materials.

Another possible method to measure the temperature in the weld zone is using an infrared pyrometer. If the operating frequency of the pyrometer is at a wavelength of high transmission

through the “transmissive” material, a signal from the surface of the “absorptive” part can be detected. To operate in this manner, the emissivity of the “transmissive” part needs to be known. Unfortunately, emissivity measurements have been found to be highly imprecise [2].

Considering the difficulty measuring the weld zone temperature, samples were assessed by three measurements. First, a visual inspection was used to observe the weld width consistency, any possible anomalies, and possible thermal decomposition. The second assessment was a destructive force test, which loads the weld in tension to the point of failure. This test is conducted in a MTS electro-mechanical loadframe using a custom grip and fixture at a displacement rate of 1.25 mm/min using a 1000 N loadcell. Finally, the width of the weld is measured with a caliper, which allows the area of the weld to be calculated and the failure strength to be determined.

A uniform looking weld that shows no sign of thermal decomposition characterizes a “good” weld. The five samples welded using the parameters developed using the design example all achieved an aesthetic “good” rating. The average force at failure

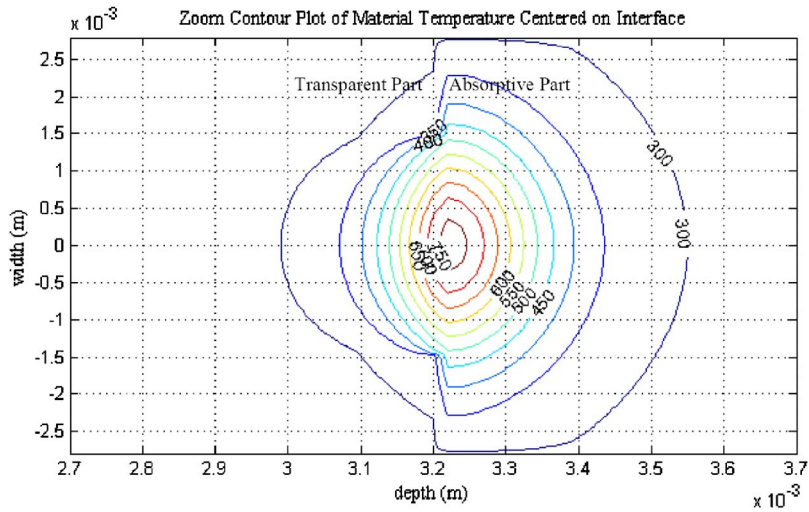


**Fig. 9** Zoomed contour plot of version 4 of the convergence study. This frame coincides with the time that the maximum weld width is achieved. The interface between the two materials occurs at  $\text{depth} = 3.2 \times 10^{-3} \text{ m}$ .

for the five samples was 609 N with a standard error of 62 N. The average measured weld width was 2.49 mm with a standard error of 0.11 mm. The weld strength for the samples was calculated by dividing the failure force by the weld width and weld length, which is a constant 19.1 mm due to the masking of the welding fixture. The average weld strength for the samples was 4.2 MPa with a standard error of 0.7 MPa. Note that the weld width of these samples was not the full width of the stem of the T, resulting in stress concentrations. These stress concentrations are affecting the calculated weld strength.

This experiment provides evidence that strongly supports the mathematical model. In the design example a 2.60 mm wide weld was predicted at the welding parameters of 17 W of laser power, a laser beam diameter of 5.7 mm, a weld velocity of 0.06 m/s, a clamping pressure of 2.0 MPa, and a surface roughness of  $1.8 \mu\text{m}$ . The error between the width predicted by the model and the width found in the experiment is 4.3%, demonstrating that the model predicted the welding conditions accurately. For reference, within the field of laser transmission welding, Becker and Potente came closest to verifying their model with findings of approximately 10–12% error, after adjusting their model based on the experimental results [2]. In the area of microwelding, Grewell and Benatar achieved similar error between their model and reported samples [8].

### Conclusion

Many current applications of LTW of thermoplastics use a trial-and-error approach to determining operating parameters. While a number of models of the welding process have been published in the literature, the agreement between models and experimental

results has been marginal at best, requiring various correction factors to be used. A prime reason that the models do not predict the process more accurately is because of the complex heat transfer that occurs when heating a polymer from ambient temperature to melt temperatures.

Starting from first principles of heat transfer, a mathematical model was created to simulate LTW. This two-dimensional model uses an energy balance method to calculate the temperature at nodes throughout the materials at specified time steps. The tem-

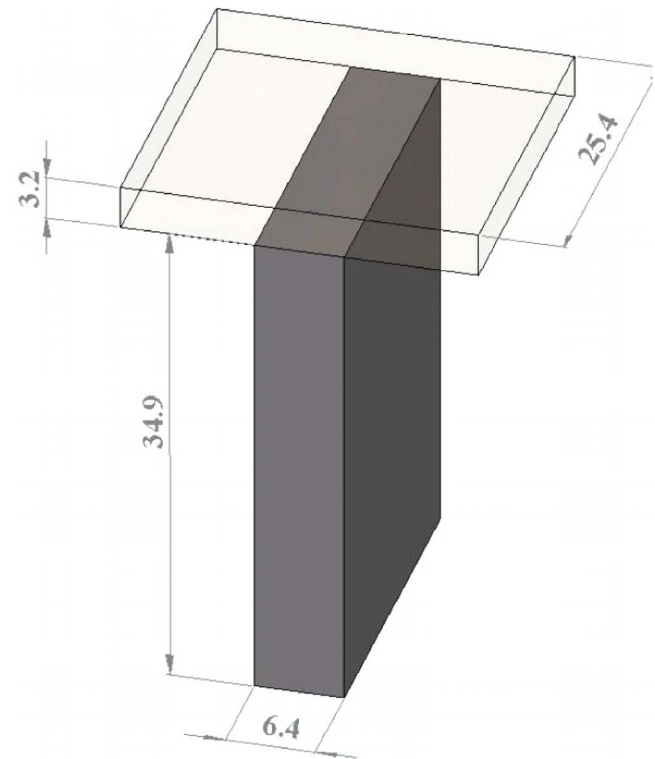


**Fig. 10** Solid model of the T-joint geometry with the associated dimensions in millimeters. Note the “transparent” part forms the top of the T, while the “absorptive” part forms the stem of the T.

**Table 3** Maximum temperature at a node located 1.25 mm away from the weld centerline on the transparent part at the interface of the two parts. Note that as the step sizes decrease, both the maximum temperature and the time that the maximum temperature occurs are converging.

Laser Welding Model: Design Example

Version	Timestep (ms)	Distance step (mm)	Maximum Temperature (K)	Time of Maximum Temperature (ms)
1	1	0.1	487.4	103.0
2	0.5	0.05	509.1	87.0
3	0.3	0.02	509.6	85.0
4	0.2	0.02	510.5	85.0

perature at each time step is solved explicitly, which does not require simultaneous equations, yet imposes stability limits on the ratio of time step size to distance step size. In addition to the temperature, the internal pressure throughout the two materials is also calculated. The pressure is important for both weld strength and thermal contact conduction between the two parts.

Knowledge of the material properties is vitally important to laser welding. Many material properties of polymers vary with temperature including: the absorption coefficient, the elastic modulus, the specific heat, the specific volume, and the thermal conductivity. The thermal contact conduction between the two parts being joined is not only a function of the temperature, but also of the pressure. The mathematical model uses these varying properties by interpolating values from "lookup" tables or solving equations that describe the property.

The purpose of the model is to allow LTW process parameters to be designed through an iterative process. Using an example, this design process is demonstrated. To improve confidence in the model, three additional refinements of the model demonstrate convergence.

Welding experiments utilizing the parameters from the design example fulfilled the purpose of validating the model. The welding samples were assessed by three methods: a visual inspection, a measurement of the failure force, and a measurement of the weld width. Not only did all of the welds result in a "good" aesthetic rating, the weld width also strongly agreed with the model. For this condition the model predicted a weld width of 2.60 mm while the average measured weld width was 2.49 mm, an error of 4.3%.

The model developed represents a new design tool that allows a LTW to be accurately designed based on the material properties of the joining materials. This design tool is possible due to creating the model from first principles and incorporating advanced topics such as thermal and optical properties changing with temperature and varying contact conduction. This allows LTW joint design to move beyond trial and error methods to a robust analytical method.

## Acknowledgment

The authors would like to thank Andersen Corporation for generously sponsoring this work. In addition, they would like to thank David Rowley for his assistance in running the welding experiments.

## References

- [1] Potente, H., Korte, J., and Becker, F., 1999, "Laser Transmission Welding of Thermoplastics: Analysis of the Heating Phase," *J. Reinf. Plast. Compos.*, **18**(10), pp. 914–920.
- [2] Becker, F., and Potente, H., 2002, "A Step Towards Understanding the Heating Phase of Laser Transmission Welding in Polymers," *Polym. Eng. Sci.*, **42**(2), pp. 365–374.
- [3] Becker, F., 2003, "Einsatz des Laserdurchstrahlenschweißens," Thesis, University of Paderborn, Paderborn, Germany.
- [4] Potente, H., and Fiegler, G., 2004, "Laser Transmission Welding of Thermoplastics-Modelling of Flows and Temperature," *Proceedings of the Society of Plastics Engineers' Annual Technical Conference*, Chicago, IL, May 16–20, 1, pp. 1193–1199.
- [5] Potente, H., and Fiegler, G., 2004, "Using Models to Describe the Joining Process," *Kunststoffe Plast Europe*, July, pp. 53–56.
- [6] Sato, K., Kurosaki, Y., Saito, T., and Satoh, I., 2002, "Laser Welding of Plastics Transparent to Near-Infrared Radiation," *Proceedings of Photon Processing in Microelectronics and Photonics*, San Jose, CA, Jan. 21–24, 4637, pp. 528–536.
- [7] Kennish, Y., Shercliff, H. R., and McGrath, G. C., 2002, "Heat Flow Model for Laser Welding of Polymers," *Proceedings of the Society of Plastics Engineers' Annual Technical Conference*, San Francisco, CA, May 5–9, 1, pp. 1132–1136.
- [8] Grewell, D., and Benatar, A., 2006, "Multi Physical Coupled Model: Predictions of Healing With Microwelding of Plastics," *Proceedings of the Society of Plastics Engineers' Annual Technical Conference*, Charlotte, NC, May 17–19, pp. 2285–2290.
- [9] Fox, M., 2001, *Optical Properties of Solids*, Oxford University Press, Oxford, UK.
- [10] Van de Ven, J., and Erdman, A., 2006, "Simultaneous Measurement of Laser Reflection and Transmission of Poly(Vinyl Chloride)," *Opt. Eng. (Bellingham)*, **45**(9), pp. 094301.
- [11] Van de Ven, J., 2006, "Laser Transmission Welding of Thermoplastics," Thesis, University of Minnesota, Twin Cities, Minneapolis, MN.
- [12] Cengel, Y. A., 1998, *Heat Transfer: A Practical Approach*, McGraw-Hill, Boston, MA.
- [13] Potente, H., Becker, F., Fiegler, G., and Korte, J., 2001, "Investigations Towards Application of a New Technique on Laser Transmission Welding," *Weld. World*, **45**(5), pp. 2–7.
- [14] Collins, E. A., Daniels, C. A., and Witenhafer, D. E., 1999, *Polymer Handbook*, Wiley, New York.
- [15] Povoletto, F., Schwartz, G., and Hermida, E. B., 1996, "Stress Relaxation of PVC Below the Yield Point," *J. Polym. Sci., Part B: Polym. Phys.*, **34**, pp. 1257–1267.
- [16] Abu-Sharkh, B. F., 2001, "Glass Transition Temperature of Poly(Vinyl Chloride) From Molecular Dynamics Simulation: Explicit Atom Model Versus Rigid CH<sub>2</sub> and CHCl Groups Model," *Comput. Theor. Polym. Sci.*, **11**(1), pp. 29–34.
- [17] Fuller, J. J., and Marotta, E. E., 2001, "Thermal Contact Conductance of Metal/Polymer Joints: An Analytical and Experimental Investigation," *J. Thermophys. Heat Transfer*, **15**(2), pp. 228–238.
- [18] Van de Ven, J., and Erdman, A., 2006, "Hot Pin Welding of Thin Polyvinyl Chloride Sheet," *J. Vinyl Addit. Technol.*, accepted.
- [19] Stokes, V. K., 2000, "Hot-Tool and Vibration Welding of Poly(Vinyl Chloride)," *J. Vinyl Addit. Technol.*, **6**(3), pp. 158–165.
- [20] Patel, K., Velazquez, A., Calderon, H. S., and Brown, G. R., 1992, "Studies of the Solid-State Thermal Degradation of PVC. I. Autocatalysis by Hydrogen Chloride," *J. Appl. Polym. Sci.*, **46**, pp. 179–187.